

Realization of Causal Representation Learning and Redefined DAG for Causal AI

Jia Li¹, Xiang Li², Xiaowei Jia³, Michael Steinbach¹, Vipin Kumar¹

University of Minnesota, ¹ Computer Science; ² Bioproducts and Biosystems Engineering. ³ University of Pittsburgh, Computer Science.

¹ {jiaxx213, stei0062, kumar001}@umn.edu, ² lixx5000@umn.edu, ³ xiaowei@pitt.edu

ABSTRACT

Causal DAG(Directed Acyclic Graph) usually lies in a 2D plane without distinguishing correlation changes and causal effects. Also, the causal effect is often approximately estimated by averaging the population's correlation changes. Now, AI(Artificial Intelligence) enables much larger-scale structural modeling, whose complex hidden confoundings make the approximation errors no longer ignorable but can snowball to considerable population-level *Causal Representation Bias*. Such bias has caused significant problems: un-generalizable causal models, unrevealed individual-level features, not utilizable causal knowledge in DL(Deep Learning), etc. In short, DAG must be redefined to enable a new framework for causal AI.

Observational time series can only reflect correlation changes in statistics. But the DL-based autoencoder can represent them as individual-level feature changes in latent space to reflect causal effects. In this paper, we introduce the redefined *do-DAG* concept and propose *Causal Representation Learning* (CRL) framework as the generic solution, along with a novel architecture to realize CRL and experimentally verify its feasibility.

KEYWORDS

Causal Representation Bias, do-DAG, Higher-Dimensional Representation, Multi-Timelines in Causality, Deep Learning.

1 INTRODUCTION

Causality is fundamental in many fields, like meteorology, biology, epidemiology, economics, etc. It aims to uncover the underlying causal relations from their observational data. Causal inference originating from classical statistics has helped to construct considerable domain knowledge in past decades[4–6]. But technical progress dramatically sped up data collecting in recent years, making it quite challenging to build Bayesian networks from large-scale data due to NP-hard. On the other hand, Machine Learning (ML) from computer science shows advanced effectiveness in handling big data on causality[15, 16, 18]. Moreover, the general success of causality ML has been considered the bedrock to realize AI [23].

Causal inference uses DAG[1] to describe data variables' associations, thus considering causal effect equivalent as their correlation change over time in time series. Figure 1 gives an example to demonstrate the bias between averaged correlations and expected standard causal effect - The elbow location defines the patient's effect rather than the days. Such a tiny bias may not cause troubles when facing small-scale data or questions. Reasonably, people in different fields greatly improved causal effect estimation using multi-variates or multi-timestep correlations [7–9]. However, it cannot be fundamentally removed. More significantly, it has blurred the population's individual-level features, leading to more intractable issues in ML, despite reducing bias for average accuracy.

A state-of-art AI application is to quantify the discrete “DAG-ness” constraint as a continuous function to realize structural optimization globally without NP-hard concern[10, 11, 37]. Designing neural network architectures according to the known DAG structure to improve DL models is straightforward. However, such neural architecture search (NAS) algorithms strangely didn't achieve general success[10, 12, 13]. The correlation-based SEMs (Sequential Equation Models) can hardly represent the individual's causal behaviors. E.g., in Figure 1, the standard effect model (i.e., black curve ends at 30 days) can be linearly generalized to fit P_1 's effect (i.e., red curve ends at 20 days), but not its correlation (ends at 30 days).

Scholkopf et al. summarized this problem as the poor generalizability of causal models[22], which recently drew attention in the ML area. They specified challenges from three perspectives: 1) Causal models often have weak robustness; 2) No mechanisms to make the learned causal knowledge reusable; 3) No universal way to model general causal knowledge from the population (i.e., the standard effect in Figure 1). They point out that “most work in causality starts from the premise that the causal variables are given” and first raised the term *Causal Representation*. Accordingly, here we name this population-level bias (caused by blurred individual-level features) as *Causal Representation Bias (CRB)*.

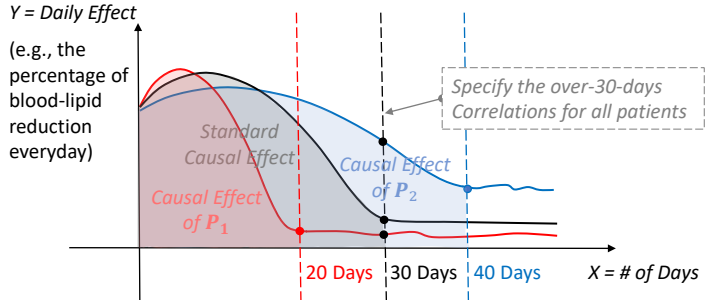


Figure 1: A medicine treats high cholesterol (i.e., blood lipid). The standard population pharmacodynamic model expects its clinical effect in 30 days by mean. A young patient P_1 spent 20 days to achieve this effect, while another older patient P_2 spent 40 days. The standard causal effect should be estimated by averaging the effects of patients but is usually approximated by averaging their over-30-days correlations.

The existence of CRB has been experimentally verified in our previous work [21] for RNN models based on clinical data. Furthermore, this paper aims to identify such CRB, analyze its forming mechanism, and summarize the critical factors. We also propose a new framework for realizing causal AI as the generic solution.

As principal contributions of this paper, we:

- Redefine *do-DAG* to identify causal effect vs. correlation change; accordingly specify the source of CRB in regular SEMs;
- Propose *Causal Representation Learning* (CRL) framework to establish do-DAG in latent space and get rid of CRB;
- Raise a novel autoencoder architecture to extract higher-dimensional representations for realizing CRL.

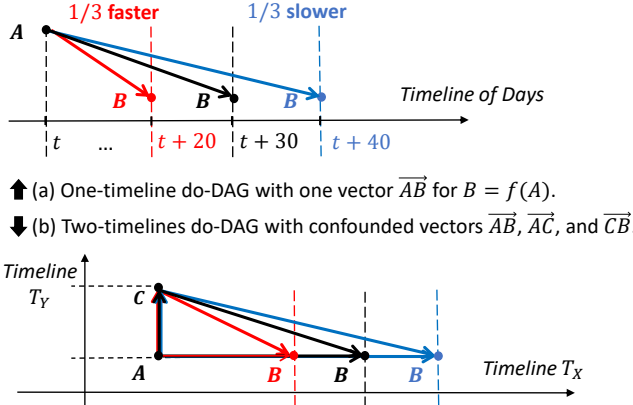


Figure 2: Edges are vectors with meaningful lengths to represent the effects' timespans according to the timeline axes.

1.1 do-DAG: the Redefined Causal DAG

In statistical causal inference, edges in DAG indicate directed pairwise causations[1], e.g., $A \rightarrow B$ from variable A to B means changing A causes B 's value change. However, this definition is inherently ambiguous – Is B an observational variable? Or the one to represent the impact of changing A ? The former refers to the *Correlation of A and B*, while the latter indicates the *Causation directed from A to B*.

According to the definition of regular SEMs (Structural Equation Models), $B = f(A)$, where function f describes the association between A 's value and B 's value with a pre-determined timespan between them. But as an observational correlation, $f(A)$ not aims to define the effect “what is B 's (must-happening) value change after A changes?”. E.g., in Figure 1, correlations = [Changes of P_1 and P_2 after 30 days], where P_1 has exceeded 100% expected medical effect but P_2 only achieved around 75%, while causal effect = [the (100%) expected change after taking medicine for any patient].

Correlations are only meaningful for estimating general features of the population but not for the individuals. For this reason, additional confounders (often hidden) are often needed to represent the individualized features. E.g., in Figure 1, the 35% effect difference between P_1 and P_2 can only be ascribed to their different body features, more than just ages.

Differentiating correlation and causation has been investigated in statistics: In *do-calculus*[2], they are represented as $B = f(A)$ and $B = f(\text{do}(A))$. In correlation $B_{t+1} = f(A_t)$, both A and B are timestamp t -dependent, and f is determined by Δt , the timespan between t and $t+1$. But $\text{do}(A)$ indicates the action of A 's changing, regardless of observational Δt , e.g., A = medicine dose, then $\text{do}(A)$ means “start to take medicine whose dose $A = 0$ is changed to $A = 1$ ”. So both $\text{do}(A)$ and $f(\text{do}(A))$ are variables valued regardless of t but represent “status”; however, they can hardly be presented statistically. Today, DL-based representation learning makes it promising.

In this paper, we redefine DAG more thoroughly as **do-DAG**, where edges only represent causations, i.e., $A \rightarrow B$ means $B = f(\text{do}(A))$, where f represents the t -independent causal effect.

Figure 2 shows two do-DAG examples. The relative timelines act as axes to indicate time-passings. Figure 2(a) corresponds to Figure 1, where A = medicine dose and B = blood lipid, then patients P_1 and P_2 can be represented as \vec{AB} stretched by different ratios along the timeline, without changing the definition of the effect function f . They can also be seen as having different speeds on the same effect: P_1 is 1/3 faster than standard, while P_2 is 1/3 slower.

Figure 2(b) has two timelines T_X and T_Y to indicate time-passings for effects \vec{AB} and \vec{AC} , respectively. \vec{AC} indicates another medicine's effect that will indirectly influence blood lipid via the third edge \vec{CB} , which forms a confounding relation over $\{A, B, C\}$ across T_X and T_Y . In this scenario, patients P_1 and P_2 have different speeds on T_X but not on T_Y . In other words, their individualized features can be represented as the different comparative ratios of two timeline-axes scales. For simplicity, we call it *individual-level heterogeneity* of the population data if everyone in it has a unique ratio.

From a geometric perspective, “stretching” the ABC -triangle along T_X can be seen as a *homography linear transformation*. And no matter whether the population data is heterogeneous (i.e., various ratios) or not, modeling the causal effects over $\{A, B, C\}$ naturally assumes the Markov condition holds for anyone.

Theorem 1. In the do-DAG space, valid SEMs must satisfy the Markov assumption, on which the Markov Decision Process (MDP) is eligible.

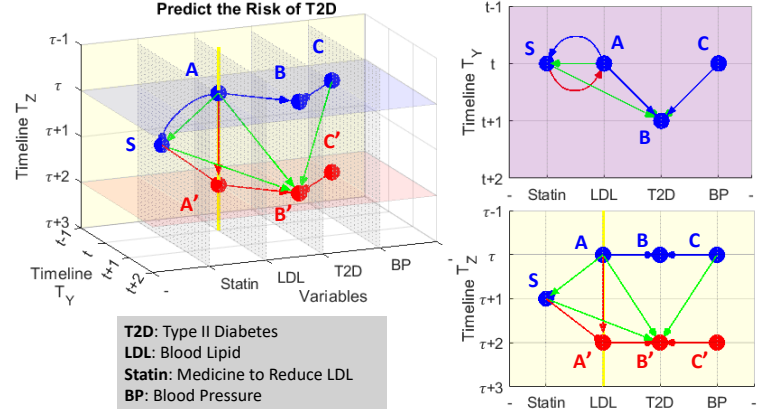


Figure 3: the 3-Dimensional do-DAG with two timelines.

1.2 CRB: the Population-Level Bias

The regular correlation-computing SEMs can lead to a population-level bias due to their violations of **Theorem 1**. Because they specify the timespans of all edges simultaneously, all individuals' comparative axes scale ratios are pre-determined to be the same. E.g., in Figure 2(b), it is like to assume the red \vec{CB} can join with black \vec{AB} at B . We name it as *Causal Representation Bias* (CRB).

Theorem 2. *Three factors lead to CRB in the regular correlation-computing SEMs: 1) Confounding, 2) across Multi-Timelines, and 3) Individual-level Heterogeneity.*

Let's use a practical scenario to demonstrate **Theorem 2**, as shown in Figure 3. This do-DAG introduces an additional axis (the X -axis) to arrange all causal variables for a better illustration, along with two timelines, T_Y , and T_Z , constructed a 3-dimensional view.

T_Y indicates the patients' disease progress in measured LDL, BP, and risk of T2D. T_Z is for medicine S 's effect. The meaning of timeline scale units is pre-determined, e.g., a step of τ on T_Z means 30 days passing to achieve S 's clinical effect, while a step of t on T_Y can be specified as a year, a month, or a week, by demand.

The use of Statin is decided by doctors based on LDL criteria ($A \rightarrow S$) and will directly reduce LDL values ($S \rightarrow A'$) and subsequently decrease the T2D risk ($A' \rightarrow B'$). The predictive SEM is $B' = f(A, S, C)$ (marked as green). But in practice, it is usually considered as $B_{t+1} = f'(A_t, S_t, C_t)$, which implies $(t+1) : (\tau+2) = 1 : 1$ for all patients in this do-DAG. If without confounding, e.g. no \overrightarrow{AS} , the modeled f' can still be generalizable by properly adjusting T_Y 's scale (in different ratios for different patients), but $\{A, S, B'\}$ confounding has determined it violates **Theorem 1** for sure.

Not intentionally, but any successful ML application has avoided at least one of the **three factors**. For instance, Markov Decision Processes (MDPs) can work well in *reinforcement learning* because most applications only involve a single timeline, e.g., playing the Go game, learning through texts, etc. Statistical causal inference is often used on structural data to deal with complex causal effects across multi-timelines, but based on domain knowledge, data can be easily de-confounded (i.e. backdoor adjustment[1]) as preprocessing. Lastly, AI can undoubtedly do a great job if some applications only need to model one object without concerns about overfitting or generalizability among different objects.

In summary, without the above theories, the existence of population-level bias CRB can hardly be investigated in practical applications. This emphasizes how significant it is to propose the do-DAG concept. Because we need an intuitive visualization of it before figuring out generic solutions for it to realize expected causal AI.

1.3 Individualization and Generalization

Mostly, AI applications for public use require the established models to be generalizable and, accordingly, able to be individualized to identify anyone in the data population. In other words, they have the same essential appeal of overcoming the individual-level heterogeneity of data, which commonly exists in many fields.

In clinical studies, learning individualized features from EHR (Electric Healthcare Records) data is quite challenging for causal inference[14]. Because collecting data samples for one patient, as many as enough to build a model, is almost impossible. On the other hand, ML is quite capable of handling big heterogeneous data to model the general causal knowledge, but due to introduced CRBs, they can hardly be robust enough to identify featured individuals.

Experiments in this paper are also based on a practical model generalization problem, which comes from the hydrology area: It is known that environmental conditions can influence the streamflow in a watershed; since physical principles are consistent on the earth, can we establish causal SEMs generalizable to any watershed? In this context, an individual is a watershed, just like a patient in EHR. However, the former can contribute plenty of observations, while the latter cannot. We can formulate these questions as below:

Suppose do-DAG G represents the general causal knowledge of a population with n individuals, then model *Individualization* means finding G_i to compare with G , and model *Generalization* means finding G_j by given G_i or G , where $i \neq j \in 1, \dots, n$; G_i and G_j are linearly transformable from G in the same do-DAG space.

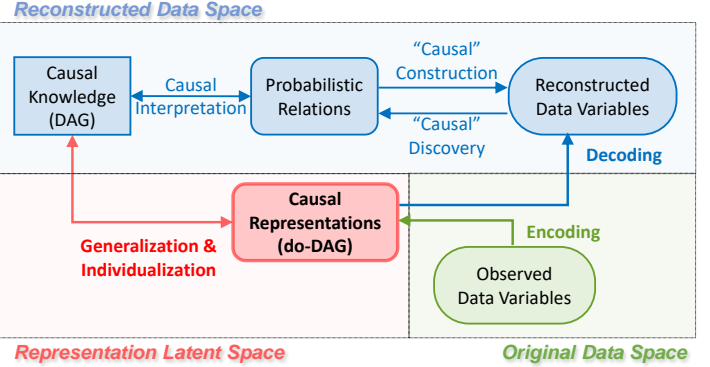


Figure 4: Proposed Causal Representation Learning (CRL) framework. Here “causal” means it is a correlation indeed.

1.4 CRL: the Proposed Framework

A generic solution for eliminating CRB is to assume the most general circumstance, where one can hardly ensure if data is heterogeneous, which effects share the same timeline, or whether unknown confounding exists. Conventionally, ML on causality can leverage domain knowledge (i.e., the known causal DAG) to improve modeling. This is equal to dealing with potential CRBs case by case but far from finding a generic solution.

The most conservative strategy to build valid SEMs for a causal structure is to model pair-wise causations (i.e. edges) one by one without making any assumptions regarding the **three factors**. Figure 4 displays the proposed framework to realize this. According to known DAG, causal effect models of all edges are established sequentially in the latent space and eventually construct the do-DAG.

To model $A \rightarrow B$, the latent space feature vectors representing A and B are extracted firstly, between which the causal effect $f(\text{do}(A))$ can be modeled (e.g. by RNNs). Connecting two edges in the latent space means “stacking” two representations. E.g. to connect $A \rightarrow B$ and $B \rightarrow C$, the feature vector of B needs to represent two roles simultaneously. Since it describes B 's status instead of observations, no matter how its value changes latently, the observational value of B in data space can always be well represented.

The term “CRL” was initially raised by Scholkopf et al.[22], focusing on some computer vision applications instead of generic concepts. But not surprisingly, their “disentangled representation” method also complies with the proposed framework.

Theorem 3. Let data matrix X augmented by all observational variables in causal graph G as the columns, the latent space for adequately representing G must have a dimensionality $\geq \text{rank}(X)$.

Theorem 3 is derived from the principle that autoencoders learn the subspace spanned by the top principal components of X [25–27], more well-known as PCA. According to it, unlike regular autoencoders to extract lower-dimensional features, we must design the higher-dimensional one from scratch (in Section 3).

There is a further hypothesis that reducing the latent space's dimensionality lower than $\text{rank}(X)$ can let the do-DAG represent G more causally (but less adequately) because it turns to stretch the latent space to be more aligned[28], which has been widely used in NLP [29, 30], and bioinformatics[31, 32]. We leave it to followers to further detect the underlying connections between them.

2 RELATED WORK

2.1 Conventional Causal Learning

Causal inference usually aims to learn the causal DAG as a Bayesian network (BN) by estimating conditional independencies among observed variables. Improvements in classical statistics are mainly in two directions. One is to determine the independencies better, including constraint-based methods (e.g., Fast Causal Inference and PC) and score-based ones (e.g., Greedy Equivalence Search) [18]. Another is to infer underlying structures from the discovered dependencies[19]. In ML, the graphical models, often presented as Structural Equation Models (SEMs) or Functional Causal Models (FCMs) [19, 20], are commonly used to leverage causal knowledge. But they are still based on DAG-indicated probabilistic dependencies without identifying causal effects from correlation changes.

In the regular correlation-computing SEMs, CRB is usually reflected as unobserved confounding, so the sufficiency assumption (i.e., no hidden confounder) is critical to decide[18]. On the other hand, statistical models prefer linearity to stay interpretable, which further confuses CRB and modeling bias.

Whether timeline is a needed variable? This is the key to distinguishing causality from correlation. Some causal questions are asking about correlations, e.g., “Does a higher smoking rate cause more lung cancers?” No matter answered by crossing 5, 10, or 30 years, it is only a parameter of correlation. But causal effects have to be described along some timelines, like “How does this medicine influence lungs (in following years)?”.

networking[11, 37], and has been further generalized into non-parametric modeling [10]. To achieve interpretability, some works attempt to reconstruct causal knowledge by properly designing architecture[13], while others try to infer dependencies directly from neuron weights[10, 11]. Such neural architecture search (NAS) methodologies aim to realize accuracy and transparency simultaneously but have not reached a general success[12].

Unlike statistical models, whose intentional de-confounding pre-processing can help prevent CRB, DL has a black-box nature, and the global optimization strategy makes it more challenging to find the inherently existing CRBs in time series. We may implicitly hope DL can automatically solve all potential biases as modeling biases, but it appears to be unrealistic[21]. The 2-dimensional causal DAGs work well for humans because we can intuitively understand the underlying timelines. But AI naturally considers all relations as associations, so we must explicitly isolate timelines as axes for AI.

3 REALIZATION METHODOLOGY OF CRL

Causal Representation Learning (CRL) models causations among the feature vectors in latent space, which are extracted by autoencoders to represent corresponding observational variables in data space. The general latent model can be interpreted as a cause model inherently[24] - Suppose variable X has an observed value x , represented as latent feature value h (with $\text{dim}(h) > \text{dim}(x)$) according to **Theorem 3**, the joint distribution $P(x, h)$ can be decomposed as $P(x|h)P(h)$, where $P(h)$ is *prior* and $P(x|h)$ is *likelihood*.

Suppose Data variables $\{X, Y, Z\}$ can be represented as feature vectors $\{\mathcal{H}, \mathcal{V}, \mathcal{K}\} \in \mathcal{R}^L$ respectively in L -dimensional latent space. Let $\mathbf{x} = [\dots, x_{t-1}, x_t]$ be a sequence of successively observed values of X , i.e., time series, whose timespan is long enough to represent the interested action $\text{do}(X)$. Accordingly, $\mathbf{h} = [\dots, h_{t-1}, h_t]$ is the corresponding sequence of feature values of \mathcal{H} in the latent space. As a regular SEM, causation $X \rightarrow Y$ is modeled by $Y = f(\text{do}(X))$ in data space, where the causal effect $f(\cdot)$ (e.g., an RNN model) is to estimate the dependence between sequence \mathbf{x} and value y_{t+1} , denoted as $P(y_{t+1} | \mathbf{x})$. Significantly, $X \rightarrow Y$ can be decomposed as causal chain $\mathbf{x} \rightarrow \mathbf{h} \rightarrow v \rightarrow y$, to reconstruct the observational dependence $P(y_{t+1} | \mathbf{x})$ as a latent dependence $P(v | \mathbf{h})$, where v is the feature value representing y_{t+1} but detached timestamp t . Let $v = f(\mathbf{h})$ model $P(v | \mathbf{h})$, then $f(\cdot)$ is the *Latent Causal Effect* model.

The ultimate goal of CRL is to build SEMs that can realize the do-DAG in latent space. “Stacking” representations is equal to stacking two (or more) latent dependencies to simulate the *posterior* distribution. E.g., given causation $X \rightarrow Y \rightarrow Z$, we are interested in the indirect causal effect from X to Z via Y , decomposed as $\mathbf{x} \rightarrow \mathbf{h} \rightarrow v \rightarrow k \rightarrow z$, where the latent vector k represents observed value z_{t+1} of Z , then what we pursue is the *posterior* $P(k | \mathbf{h}) = P(k | v)|_{v=f(\mathbf{h})}$. Given f is ready, we only need to estimate the latent model $g(\cdot)$, such that $k = g(v)|_{v=f(\mathbf{h})}$, by stacking the target dependence $P(k | v)$ onto the modeled dependence $P(v | \mathbf{h})$. Notably, training $g(\cdot)$ for $k = g(v)$ and $k = g(v)|_{v=f(\mathbf{h})}$ are two different processes. The former is modeling $Y \rightarrow Z$ rather than $X \rightarrow Y \rightarrow Z$ as the latter, with different input data streams. From the autoencoder's perspective, let \mapsto be the notation connecting its input and output distributions in latent space; the former has $P(v) \mapsto P(k)$ while the latter has $P(v|h) \mapsto P(k)$.

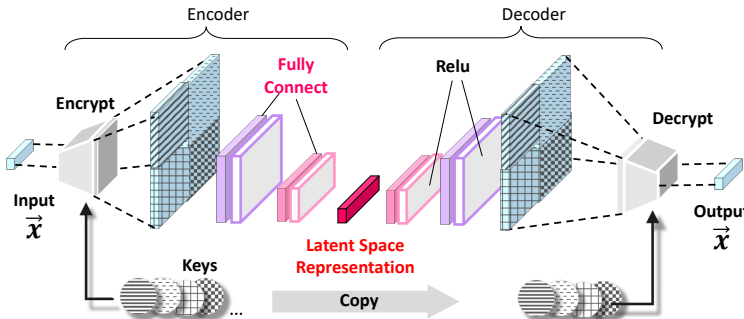


Figure 5: Proposed architecture of the higher-dimensional representation extraction autoencoder.

2.2 Deep Learning in Causality

Deep Learning (DL) can handle non-linear and higher-order dependencies among variables and simultaneously provide global solutions, so it is trending to leverage its effectiveness and the interpretability of causal inference[12]. A significant contribution is converting the discrete combinational constraints on DAG's “acyclicity” into continuous ones to realize the global optimization on

We start by proposing a novel architecture to extract higher-dimensional representations (3.1), along with the critical layers' design (3.2); then, demonstrate the methods of learning latent causal effects and stacking representations (3.3); lastly, introduce causal discovery algorithm based on do-DAG in latent space (3.4).

3.1 Autoencoder Architecture

Ordinary autoencoders aim to extract lower-dimensional features to represent some objects having numerous high-dimensional data samples, e.g. many images with millions of pixels, which is more like a distillation process. But we need to reconstruct some low-dimensional data variables as higher-dimensional feature vectors in one latent space, in which their latent dependencies can be estimated later. **Theorem 3** is to emphasize that such latent space should provide sufficient freedom for all possible latent causal effects modeling. We temporarily shelve further discussions about its dimensionality choosing boundaries but only focus on this paper's experiments. We have 10 observational data variables whose dimensions are between 1 ~ 5 and are summarized as 32 (refer to Table 2). We initially set up a 64-dimensional latent space, but it turned out to be highly redundant because of solid associations among variables, finally reduced to 16-dimensional.

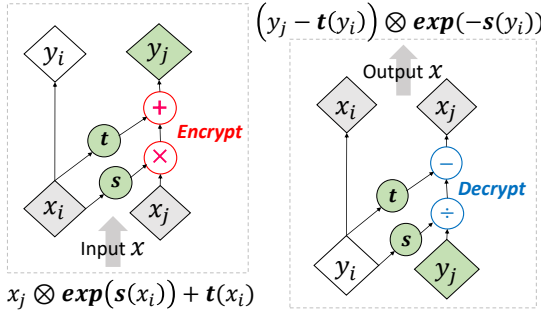


Figure 6: Encrypt and Decrypt with specified $s(\cdot)$ and $t(\cdot)$.

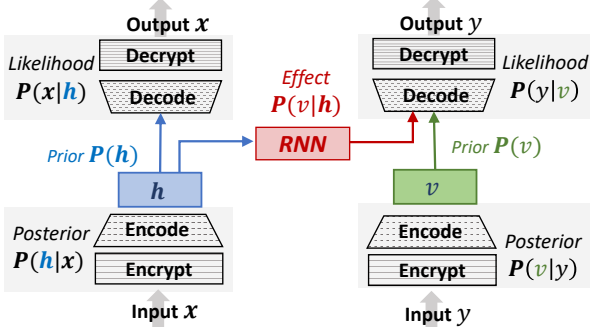


Figure 7: Architecture of learning latent causal effect $v = f(h)$.

The proposed autoencoder architecture is shown in Figure 5, with a pair of initially designed symmetric layers, *Encrypt* and *Decrypt*, added at *Input* and *Output*, respectively. Here we denote the observed value x as $\vec{x} \in \mathcal{R}^d$, i.e., a vector consists of d digits, for better interpretation. The *Encrypt* works as a “feature amplifier” to extract higher-order features from the input vector \vec{x} to extend its length, which will be recovered to its original format by *Decrypt*.

In other words, such an extension process has to be *Invertible* to ensure the reconstruction accuracy for \vec{x} .

A *double-wise* extension is to encrypt every two digits in \vec{x} as a new digit to reflect their association. Specifically, encrypt is by a *Key*, which is a group of constants generated by the Encoder. The Decoder copies this *Key* to decrypt it into the two digits inversely. With multiple *Keys*, we can have different extensions for the same input, and concatenating them all together can form a much longer new vector than the original one. By one *Key*, \vec{x} can be extended to be a $(d-1)*(d-1)$ length new vector - For convenience, we display it as a square in Figure 5 (not implying a 2-dimensional vector) with patterned grids as the *Key*'s “signature”. By four different *Keys*, we can get four squares with different signatures, which means a $4*(d-1)*(d-1)$ length extended input vector for \vec{x} .

As a metaphor, the *Key* works like a filter in regular autoencoders. According to demand, one can realize higher-order extension in the same way, e.g., a *triple-wise* one over three digits.

3.2 Encrypt and Decrypt Layers

Let the observed value $x = (x_1, x_2, \dots, x_d)$ has d digits. The *double-wise* extension in Encrypt is to realize a transformation on digit pair (x_i, x_j) , represented as $f_\theta(x_i, x_j)$, where $i \neq j \in 1, \dots, d$, and parameter $\theta = (w_s, w_t)$ specifies the *Key*, consisting of two weights to define two elementary functions $s(\cdot)$ and $t(\cdot)$. Let $f_\theta(x_i, x_j) = x_j \otimes \exp(s(x_i)) + t(x_i)$, where \otimes denotes the element-wise multiplication. As shown in the left side of Figure 6, the new digit $y_j = f_\theta(x_i, x_j)$ can be seen as encrypting x_j to be y_j by using x_i as a parameter. Symmetrically, the inverted function f_θ^{-1} in Decrypt is $(y_j - t(y_i)) \otimes \exp(-s(y_i))$. Since calculating f_θ^{-1} does not involve inverted function s^{-1} or t^{-1} , the two elementary functions can be either linear or non-linear by the demand to realize linear or non-linear transformations. Let's assemble all f_θ as $\mathcal{F}(X; \Theta)$ about data variable X , where Θ is the set of all θ . Then the two layers, Encrypt and Decrypt, can be denoted as $Y = \mathcal{F}(X; \Theta)$ and $X = \mathcal{F}^{-1}(Y; \Theta)$ respectively. It is worth highlighting that the work of Dinh, L. et al. [38] inspires the proposed design above. Our source code is provided as in a complete demo¹.

3.3 Latent Causal Effects

Figure 7 displays the two-autoencoders architecture of estimating latent dependence $P(v|h)$ as an RNN model $v = f(h)$. The established tuple $(\mathcal{H}, \mathcal{V}, f)$ can fully represent observational causation $X \rightarrow Y$, where $\mathcal{H}, \mathcal{V} \in \mathcal{R}^L$ represent X and Y individually, and the modeled f represents the causal effect from X to Y .

\mathcal{H} and \mathcal{V} were initialized as two independent feature vectors in the same \mathcal{R}^L space, extracted by the proposed autoencoder architecture. When learning f , their feature values keep changing as they are “moving” closer to each other and optimally minimizing their distance, while f is like the bridge to cross this distance. There are three optimizations exist in each iteration:

- (1) For \mathcal{H} : update $P(h|x)$ and $P(x|h)$, optimize X reconstruction.
- (2) For f : update $P(h|x)$, $P(v|h)$ and $P(y|v)$, optimize causal effect reconstruction.
- (3) For \mathcal{V} : update $P(v|y)$ and $P(y|v)$, optimize Y reconstruction.

¹https://github.com/kfljlia/bijective_crossing_functions/blob/main/code_bicross_extractor.py

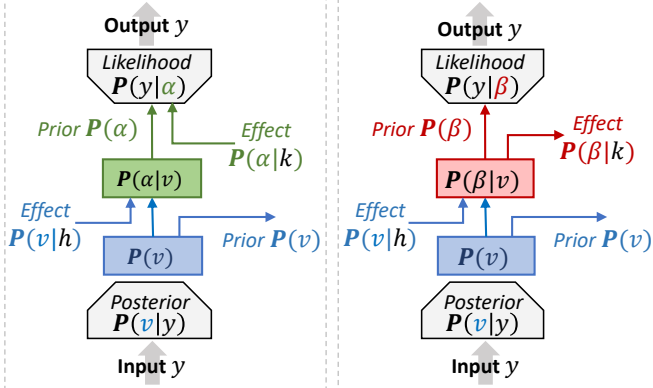


Figure 8: Ways of stacking two representations on Y . Left: stacking \overrightarrow{XY} with \overrightarrow{ZY} . Right: stacking \overrightarrow{XY} with \overrightarrow{YZ} .

“Stacking” two representations on one data variable in latent space means changing its feature vector’s value to make it represent two roles simultaneously. E.g., the learning process in Figure 7 contains two stacking operations: One is to stack X with \overrightarrow{XY} by changing \mathcal{H} ’s value, and another is to stack Y with \overrightarrow{XY} by changing \mathcal{V} ’s value, given that \mathcal{H} and \mathcal{V} have been initially established as the representations of X and Y individually.

Figure 8 shows the scenarios of stacking two edges’ representations among three variables. From the autoencoder’s perspective, all input and output data streams reflect distributions without distinguishing if they are sequences, so only the single value notations are used here. Given that the \overrightarrow{XY} effect has been well-established to input distribution $P(v|h)$, the left architecture is to establish $X \rightarrow Y \leftarrow Z$ while the right one is for $X \rightarrow Y \rightarrow Z$. To preserve all representations established, such stacking is realized by adding one more representation layer. So this operation can be easily rollbacked by removing the corresponding layer from the architecture.

Multiple representation layers in one autoencoder can make it very flexible to realize different combinational input and output distributions. E.g., for the left side architecture of Figure 8, $P(v|h) \mapsto P(\alpha)$ is to represent $X \rightarrow Y$, and input $P(\alpha|k)$ is to represent $Z \rightarrow Y$. For the right side one, $P(v) \mapsto P(\beta|k)$ is to realize $Y \rightarrow Z$ effect with Y input, while $P(v|h) \mapsto P(\beta|k)$ means $X \rightarrow Y \rightarrow Z$.

If based on domain knowledge, the structural do-DAG can be established gradually by stacking the estimated effects of edges sequentially, according to the known causal DAG. On the other hand, one can also use the same method to perform causal structure discovery in the latent space by detecting possible edges among the initialized feature vectors representing data variables.

3.4 Discovery Algorithm in Latent Space

Suppose a group of feature vectors has been established respectively in the \mathcal{R}^L latent space to represent corresponding data variables. Algorithm 1 demonstrates the heuristics discovery procedure by using KLD (KL-Divergence) as the metric to evaluate the detected edges’ causal strengths. KLD is to estimate the similarity of the effect model’s output and the initialized (as the ground truth) feature representation of the resulted variable of an edge. Briefly, it is to compare the RNN’s output $P(v|h)$ and the *prior* $P(v)$ in Figure 7.

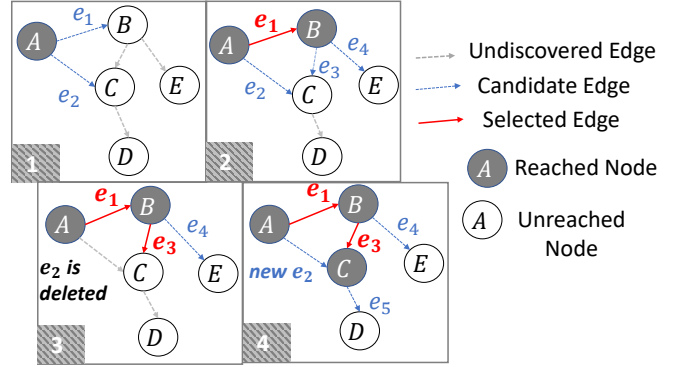


Figure 9: Example of Causal Discovery in the latent representation space. Nodes indicate representation vectors.

The lower KLD means better similarity, thus indicating a higher causal strength. Besides, MSE is a conventionally used evaluation, but considering that data variances may dominate it [35, 36], we choose to stick with KLD and use MSE as a side metric. For simplicity, in the following, for edge $A \rightarrow B$, we call variables A and B as the *cause node* and *result node*, respectively.

An illustrative example of the latent space causal discovery is shown in Figure 9. In these four consecutive steps, edge e_1 and edge e_3 are selected one after another. The selection of e_1 makes node B reachable as the start node of e_3 . At step 3, the learned causal effect of e_2 , from A to C , is deleted from the candidate edges and needs to be recalculated because edge e_3 has reached C and changed current causal conditions on C .

Algorithm 1: Latent Causal Discovery with KLD Metric

```

Result: ordered edges set  $E = \{e_1, \dots, e_n\}$ 
 $E = \{\}$ ;
 $N_R = \{n_0 \mid n_0 \in N, \text{Parent}(n_0) = \emptyset\}$ ;
while  $N_R \subset N$  do
   $\Delta = \{\}$ ;
  for  $n \in N$  do
    for  $p \in \text{Parent}(n)$  do
      if  $n \notin N_R$  and  $p \in N_R$  then
         $e = (p, n)$ ;
         $\beta = \{\}$ ;
        for  $r \in N_R$  do
          if  $r \in \text{Parent}(n)$  and  $r \neq p$  then
             $\beta = \beta \cup r$ 
          end
        end
         $\delta_e = K(\beta \cup p, n) - K(\beta, n)$ ;
         $\Delta = \Delta \cup \delta_e$ ;
      end
    end
  end
   $\sigma = \text{argmin}_e (\delta_e \mid \delta_e \in \Delta)$ ;
   $E = E \cup \sigma$ ;
   $N_R = N_R \cup n_\sigma$ ;
end

```

$G = (N, E)$	graph G consists of nodes set N and edges set E
N_R	the set of reachable nodes
E	edges in order of being discovered
$K(\beta, n)$	KLD metric between the causes set β and effect node n
$\Delta = \{\delta_e\}$	the set of all KLD Gain δ_e for each candidate edge e
n, p, r	notation of node
e, σ	notation of edge

4 FEASIBILITY EXPERIMENTS

The feasibility experiments are designed to verify that the proposed autoencoder architecture can effectively perform higher-dimensional representation extractions, and accordingly, we can establish the causal effects estimations successively in the latent space. Eventually, we aim to completely build up the graphical causal structure of do-DAG, based on which the general causal discovery and construction processes can be accurately performed.

The adopted experimental data is a professional synthetic hydrology dataset, with the learning task of forecasting streamflow by given observed environmental conditions (e.g., temperature and precipitation). The purpose of performing causal representation learning (CRL) on this hydrology data is to realize causal model generalization among different watersheds, such that the causal model established on the dataset X_1 collected from watershed No.1, can be calibrated to fit the dataset X_2 from watershed No.2. This application is motivated by sharing common knowledge across different data qualities. For example, X_1 is qualified enough to establish a complete graphical causal model, but X_2 does not. It has been known that their underlying hydrological schemes are very similar (e.g., geographical positions are closed), but because of various unmeasurable conditions (e.g., different economic developments and land use), directly applying X_1 's model on X_2 performs poorly. Moreover, the existing causal models are based on physical modules with limited parameters. Thus these models' degree of freedom is far from being able to do calibrations on low-qualification data.

Because of space limitations, we can only demonstrate the CRL modeling performances (with demo²) without experimental comparisons for evaluating generalization in this paper. In future works, we plan to realize both the individualization and generalization of CRL models. Besides, due to empirical restrictions, we are out of access to EHR data for this work; for proof of causal representation bias (CRB) in EHR, please refer to our previous work [21].

4.1 Hydrology Dataset

SWAT (Soil & Water Assessment Tool) is a professional hydrology data simulation system is commonly used to generate synthetic datasets or calibrate realistic data samples based on physical modules. Our experiments are based on the synthetic data generated by the SWAT system, for simulating the Root River Headwater watershed in Southeast Minnesota. From this dataset, we selected 60 successive virtual years with a daily update frequency. The performances are mainly evaluated as the accuracies of unsupervised data reconstruction via the proposed CRL model.

The hydrology system entails water fluxes and states across the earth's space, such as snowpack melting, evapotranspiration, and soil moisture. Its underlying causality is highly complex, exhibits nonlinearities, and contains a lot of unobservable dependencies. In recent years, machine learning on causal inferences naturally attracted hydrologists' attention [33]; DL-based methods are widely used to efficiently extract representations from time series. As a typical application, RNN models contribute state-of-the-art techniques for streamflow prediction [34]. Here, the word "streamflow"

Table 1: Explanations of the nodes in Figure 10

ID	Variable Name	Explanation
A	Environmental set I	Wind Speed + Humidity + Temperature
B	Environmental set II	Temperature + Solar Radiation + Precipitation
C	Evapotranspiration	Evaporation and transpiration
D	Snowpack	The winter frozen water in the ice form
E	Soil Water	Soil moisture in vadose zone
F	Aquifer	Groundwater storage
G	Surface Runoff	Flowing water over the land surface
H	Lateral	Vadose zone flow
I	Baseflow	Groundwater discharge
J	Streamflow	Sensors recorded outputs

refers to a critical statement variable in hydrologic processes, observed by numerous monitors in the water body and influenced by comprehensive physical factors over months.

Figure 10 displays the ground truth graphical causal relationship used by SWAT to generate synthetic data based on current hydrology knowledge. Explanations about the nodes are listed in Table 1. The causal strengths of these routines are determined by their present contributions to output streamflow, remarked by different colors. The hydrological interpretation is that the surface runoff routine (1st tier causality) cause streamflow peaks more quickly than the lateral flow routine (2nd tier causality), which is more critical than the baseflow dynamics (3rd tier causality).

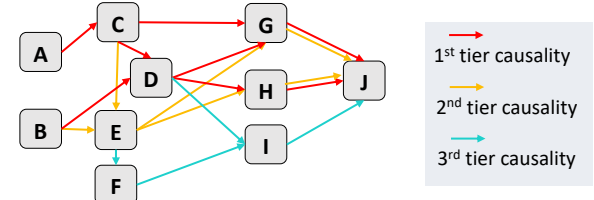


Figure 10: The underlying causal graph from current hydrology knowledge. The reducing expert-expected causal strengths define the tiers of causal routines.

4.2 Autoencoder Reconstruction Test

The proposed higher-dimensional representation extraction autoencoder is used on each node in Figure 10. Accordingly, 10 vectors have been extracted in the latent space to represent the nodes from A to J, respectively. The major challenge comes from the low dimensionality of the original data variables. As shown in Table 2, their maximal length only reaches 5, and the prediction target, node J, is just a one-column variable. We first expand each variable to have a new length of 12 by randomly repeating their columns, then augmented with 12-dimensional dummy variables of months to form 24-dimensional input variables. In the double-wise amplifications, every column has been extracted 23 times and augmented with itself. This way, we obtain a 576-dimensional output through the *Encrypt* process. And the representation is set to be 16-dimensional.

Table 2 shows each variable's statistics characteristics and the reconstruction performance (comparing the output and input of the autoencoder) evaluated by RMSE, where less RMSE indicates higher accuracy. We provide two RMSE evaluations for each variable in

²https://github.com/kflijia/bijective_crossing_functions.git

Table 2: Performance of Autoencoder Reconstruction.

Variable	Length	Mean	Std	Min	Max	Non-Zero Rate%	RMSE on Scaled	RMSE on Original	BCE of Mask
A	5	1.8513	1.5496	-3.3557	7.6809	87.54	0.093	0.871	0.095
B	4	0.7687	1.1353	-3.3557	5.9710	64.52	0.076	0.678	1.132
C	2	1.0342	1.0025	0.0	6.2145	94.42	0.037	0.089	0.428
D	3	0.0458	0.2005	0.0	5.2434	11.40	0.015	0.679	0.445
E	2	3.1449	1.0000	0.0285	5.0916	100	0.058	3.343	0.643
F	4	0.3922	0.8962	0.0	8.6122	59.08	0.326	7.178	2.045
G	4	0.7180	1.1064	0.0	8.2551	47.87	0.045	0.81	1.327
H	4	0.7344	1.0193	0.0	7.6350	49.93	0.045	0.009	1.345
I	3	0.1432	0.6137	0.0	8.3880	21.66	0.035	0.009	1.672
J	1	0.0410	0.2000	0.0	7.8903	21.75	0.007	0.098	1.088

Table 3: Brief Summary of the Latent Causal Discovery Results.

Edge	A→C	B→D	C→D	C→G	D→G	G→J	D→H	H→J	B→E	E→G	E→H	C→E	E→F	F→I	I→J	D→I
KLD	7.63	8.51	10.14	11.60	27.87	5.29	25.19	15.93	37.07	39.13	39.88	46.58	53.68	45.64	17.41	75.57
Gain	7.63	8.51	1.135	11.60	2.454	5.29	25.19	0.209	37.07	-5.91	-3.29	2.677	53.68	45.64	0.028	3.384

the scaled (i.e., normalized) and original values. The characteristic columns are calculated as scaled values.

It is worth mentioning that the hydrology dataset contains a large number of meaningful zero values. For example, the variable *D*, named Snowpack, only has non-zero values in winter, whose water body will present as Soil Water (variable *E*) in the other seasons. However, the zeros do have meanings since they represent the variables vanishing. Therefore, we perform double reconstructions simultaneously in the autoencoder: one for the variable’s continuous values, and the other to be the non-zero indicator, evaluated by BCE and named Mask in the table. The RMSE performances in Table 2 are obtained by multiplying these two results. The percentage of non-zero values is also provided for each node. These shallow RMSE values indicate the success of the reconstruction processes, which are in the range of [0.01, 0.09], except node *F*, the Aquifer variable. It has been known that the aquifer system modeling is still premature in the present hydrology area. So this is reasonable to infer that in the synthetic data, Aquifer is closer to random noise than other variables.

4.3 Latent Causal Effects Learning Test

The latent causal effect learning is evaluated on pair-wise causations. And by stacking them, we successfully recover the ground truth graphical causal structure displayed in Fig 10. To compare the changing of the reconstructing performance by each stacking, we construct the Table 4 for each variable that has ever been the *result* node of pair-wise causations. For example, node *G* has three possible causes *C*, *D*, and *E*, so we can build four causal effect models in total: the individual pair-wise causations *C*→*G*, *D*→*G*, *E*→*G*, and the stacked causal effects *CDE*→*G*. For convenience, we call them “*pair-effect*” and “*stacking-effect*” respectively in the following. In Table 4, we also list the initial reconstruction performance for each variable, as the comparison baseline, in the column named “Variable Reconstruction (initial performance)”.

There are three different optimization tasks in the latent causal effect learning process (refer to Section 3.3), among which both the *second* and *third* one are about the *result* node. Therefore, in Table 4, we give out the performances of these two roles for each node:

the role in the *third* optimization is shown as the columns named “Variable Reconstruction (as result node)”; and the role of the *second* one is in the columns named “Latent Causal Effect Reconstruction”, which represent the causal effect learning performances of RNN models, along with the KLD metrics to display the learned causality strength (the lower is stronger).

The KLD metric differences among variables are easy to be observed. Variable *J* has the smallest KLD values, which means that *G* (Surface Runoff), *H* (Lateral), and *I* (Baseflow) significantly cause *J* (Streamflow). While the weaker causal relations present as higher values of KLD. For example, variable *I* can hardly be predictable given *D* and *F*. For *result* nodes, *D*, *E*, *J*, the *stacking-effect* causal strength is in the intermediate range of *pair-effect* strength, which implies that the internal associative relationship inside their cause nodes is ambiguous. For *G* and *H*, the *stacking-effect* causal strength KLD is lower than all the *pair-effect* ones. It is reasonable to infer that the *stacking-effect* model has captured additional causal information from the associative relationships among their causes nodes. Besides, the KLD metric also tells which cause node contributes the most to the latent causal effect. For example, *C*→*G* strength is closer to *CDE*→*G* than the other causes nodes, which indicates *C* to be the strongest source in this causal effect.

To better present the reconstruction performances of the stacked causal structure, we illustrate their results as data simulations in Figure 11, which includes three different nodes, *J*, *G*, and *I* in the same synthetic year. For each node, the initial variable reconstruction performance is plotted as the blue line, and all the latent causal effects we have learned are displayed in different colors. Besides RMSE, here we also use another metric, NSE (Nash–Sutcliffe model efficiency coefficient) to be the hydrology-meaningful accuracy evaluation, where NSE = 1 defines the best prediction. The three initial variable reconstructions (blue lines) in Figure 11 almost reach the best performance, as they overlapped with the ground truth observations (black dots). The red lines indicate simulations from *stacking-effect*, whose performances are highly consistent with our analysis above: Node *J* has the best prediction; node *I* can hardly be predictable; and node *G* is predicted best by *CDE* causes combination, among which *C* provides the strongest causality.

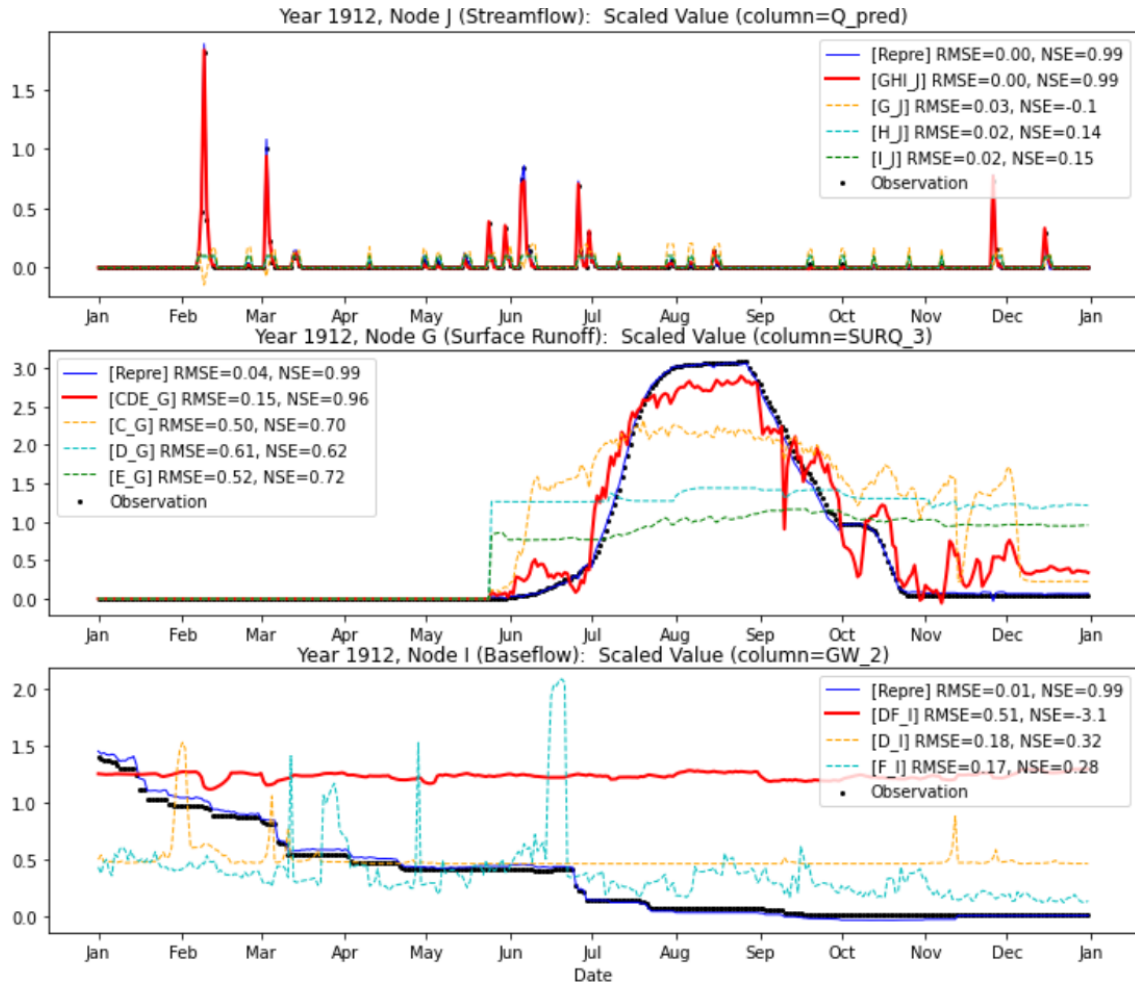


Figure 11: Performance of Latent Causal Effect Reconstruction Examples. (evaluated as data simulation accuracy)

4.4 Causal Structure Discovery Test

The latent causal discovery is based on the KLD causality strength evaluation. 3 displays the edges' discovered order and their corresponding KLD and KLD-Gains. Here the table cells are colored according to the different tiers of causality, consistent with the ground truth shown in Figure 10. Since the discovery algorithm successfully distinguished the 3 tiers, the proposed KLD metric has been proven to work effectively.

Due to limited space, the results in Table 3 is only a brief version, whose complete version is provided in Appendix A Table 1, which includes all results during the causal discovery, organized by the round of detection. As a baseline comparison, we also performed the conventional FGES (fast greedy equivalence search) causal discovery method in 10 cross-validation. Their results are given in Appendix A Table 2, with apparently worse performance than the proposed CRL method.

5 CONCLUSION

Understanding about timeline is a fundamental difference between humans and AI, which can also help to differentiate causation from correlation. The 2-dimensional causal DAG does not distinguish

causal effect and correlation change, thus only eligible as the awareness model for humans but unsuitable to direct AI's learning. This paper systematically analyzed the scheme of significant population-level bias in causal AI, based on the redefined do-DAG concept, and also realized a new general framework to solve it.

In recent years, AI applications like ChatGPT appear to be very impressive. But we barely hear AI can replace humans in complicated decisions. AI's capability is like "sealed" on causally structured data's learning. We hope this work can help to lead the next trend.

REFERENCES

- [1] Pearl, Judea. *Causal inference in statistics: An overview*. (2009): 96-146.
- [2] Pearl, Judea. *The do-calculus revisited*. arXiv preprint arXiv:1210.4852 (2012).
- [3] Scheines, Richard. *An introduction to causal inference*. (1997).
- [4] Wood, Christopher J., and Robert W. Spekkens. *The lesson of causal discovery algorithms for quantum correlations: Causal explanations of Bell-inequality violations require fine-tuning*. New Journal of Physics 17.3 (2015): 033002.
- [5] Vuković, Matej, et al. *Causal Discovery in Manufacturing: A Structured Literature Review*. Journal of Manufacturing and Materials Processing 6.1 (2022): 10.
- [6] Ombadi, Mohammed, et al. *Evaluation of methods for causal discovery in hydro-meteorological systems*. Water Resources Research 56.7 (2020): e2020WR027251.
- [7] Guyon, Isabelle. *Practical feature selection: from correlation to causality*. Mining massive data sets for security (2008): 27-43.
- [8] Zhao, Liping. *The gut microbiota and obesity: from correlation to causality*. Nature Reviews Microbiology 11.9 (2013): 639-647.

Table 4: The latent causal effect learning performances.

Variable	Variable Reconstruction (initial performance)			Cause Node	Variable Reconstruction (as result node)			Latent Causal Effect Reconstruction			
	RMSE on Scaled Values	RMSE on Original Values	BCE Mask		RMSE on Scaled Values	RMSE on Original Values	BCE Mask	RMSE on Scaled Values	RMSE on Original Values	BCE Mask	KLD (in latent space)
C	0.037	0.089	0.428	A	0.0295	0.0616	0.4278	0.1747	0.3334	0.4278	7.6353
D	0.015	0.679	0.445	BC	0.0350	1.0179	0.1355	0.0509	1.7059	0.1285	9.6502
				B	0.0341	1.0361	0.1693	0.0516	1.7737	0.1925	8.5147
				C	0.0331	0.9818	0.3404	0.0512	1.7265	0.3667	10.149
E	0.058	3.343	0.643	BC	0.4612	26.605	0.6427	0.7827	45.149	0.6427	39.750
				B	0.6428	37.076	0.6427	0.8209	47.353	0.6427	37.072
				C	0.5212	30.065	1.2854	0.7939	45.791	1.2854	46.587
F	0.326	7.178	2.045	E	0.4334	8.3807	3.0895	0.4509	5.9553	3.0895	53.680
G	0.045	0.81	1.327	CDE	0.0538	0.9598	0.0878	0.1719	3.5736	0.1340	8.1360
				C	0.1057	1.4219	0.1078	0.2996	4.6278	0.1362	11.601
				D	0.1773	3.6083	0.1842	0.4112	8.0841	0.2228	27.879
				E	0.1949	4.7124	0.1482	0.5564	10.852	0.1877	39.133
H	0.045	0.009	1.345	DE	0.0889	0.0099	2.5980	0.3564	0.0096	2.5980	21.905
				D	0.0878	0.0104	0.0911	0.4301	0.0095	0.0911	25.198
				E	0.1162	0.0105	0.1482	0.5168	0.0097	3.8514	39.886
I	0.035	0.009	1.672	DF	0.0600	0.0103	3.4493	0.1158	0.0099	3.4493	49.033
				D	0.1212	0.0108	3.0048	0.2073	0.0108	3.0048	75.577
				F	0.0540	0.0102	3.4493	0.0948	0.0098	3.4493	45.648
J	0.007	0.098	1.088	GHI	0.0052	0.0742	0.2593	0.0090	0.1269	0.2937	5.5300
				G	0.0077	0.1085	0.4009	0.0099	0.1390	0.4375	5.2924
				H	0.0159	0.2239	0.4584	0.0393	0.5520	0.4938	15.930
				I	0.0308	0.4328	0.3818	0.0397	0.5564	0.3954	17.410

[9] Marwala, Tshilidzi. *Causality, correlation and artificial intelligence for rational decision making*. World Scientific, 2015.

[10] Zheng, Xun, et al. *Learning sparse nonparametric dags*. International Conference on Artificial Intelligence and Statistics. PMLR, 2020.

[11] Lachapelle, Sébastien, et al. *Gradient-based neural dag learning*. arXiv preprint arXiv:1906.02226 (2019).

[12] Luo, Yunan, Jian Peng, and Jianzhu Ma. *When causal inference meets deep learning*. Nature Machine Intelligence 2.8 (2020): 426-427.

[13] Ma, Jianzhu, et al. *Using deep learning to model the hierarchical structure and function of a cell*. Nature methods 15.4 (2018): 290-298.

[14] Qayyum, Adnan, et al. *Secure and robust machine learning for healthcare: A survey*. IEEE Reviews in Biomedical Engineering 14 (2020): 156-180.

[15] Ahmad, Muhammad Aurangzeb, Carly Eckert, and Ankur Teredesai. *Interpretable machine learning in healthcare*. Proceedings of the 2018 ACM international conference on bioinformatics, computational biology, and health informatics. 2018.

[16] Sanchez, Pedro, et al. *Causal machine learning for healthcare and precision medicine*. Royal Society Open Science 9.8 (2022): 220638.

[17] Crown, William H. *Real-world evidence, causal inference, and machine learning*. Value in Health 22.5 (2019): 587-592.

[18] Sobel, Michael E. *An introduction to causal inference*. Sociological Methods & Research 24.3 (1996): 353-379.

[19] Glymour, Clark, Kun Zhang, and Peter Spirtes. *Review of causal discovery methods based on graphical models*. Frontiers in genetics 10 (2019): 524.

[20] Elwert, Felix. *Graphical causal models*. Handbook of causal analysis for social research (2013): 245-273.

[21] Li, Jia, et al. *Teaching deep learning causal effects improves predictive performance*. arXiv preprint arXiv:2011.05466 (2020).

[22] Schölkopf, Bernhard, et al. *Toward causal representation learning*. Proceedings of the IEEE 109.5 (2021): 612-634.

[23] Li, Yunzhu, et al. *Causal discovery in physical systems from videos*. Advances in Neural Information Processing Systems 33 (2020): 9180-9192.

[24] Bengio, Yoshua, et al. *Unsupervised feature learning and deep learning: A review and new perspectives*. CoRR, abs/1206.5538 1.2665 (2012): 2012.

[25] Baldi, Pierre, and Kurt Hornik. *Neural networks and principal component analysis: Learning from examples without local minima*. Neural networks 2.1 (1989): 53-58.

[26] Plaut, Elad. *From principal subspaces to principal components with linear autoencoders*. arXiv preprint arXiv:1804.10253 (2018).

[27] Wang, Yasi, Hongxun Yao, and Sicheng Zhao. *Auto-encoder based dimensionality reduction*. Neurocomputing 184 (2016): 232-242.

[28] Jain, Saachi, Adityanarayanan Radhakrishnan, and Caroline Uhler. *A mechanism for producing aligned latent spaces with autoencoders*. arXiv:2106.15456 (2021).

[29] Pennington, Jeffrey, Richard Socher, and Christopher D. Manning. *Glove: Global vectors for word representation*. Proceedings of the 2014 conference on empirical methods in natural language processing (EMNLP). 2014.

[30] Rong, Xin. *word2vec parameter learning explained*. arXiv:1411.2738 (2014).

[31] Belyaeva, Anastasiya, et al. *Causal network models of SARS-CoV-2 expression and aging to identify candidates for drug repurposing*. Nature comm 12.1 (2021): 1024.

[32] Lotfollahi, Mohammad, F. Alexander Wolf, and Fabian J. Theis. *scGen predicts single-cell perturbation responses*. Nature methods 16.8 (2019): 715-721.

[33] Goodwell, Alison E., et al. *Debates—Does information theory provide a new paradigm for Earth science? Causality, interaction, and feedback*. Water Resources Research 56.2 (2020): e2019WR024940.

[34] Kratzert, Frederik, et al. *Rainfall-runoff modeling using long short-term memory (LSTM) networks*. Hydrology and Earth System Sciences 22.11 (2018): 6005-6022.

[35] Reisach, Alexander G., et al. *Beware of the simulated dag! varsorability in additive noise models*. arXiv:2102.13647 (2021).

[36] Kaiser, Marcus, and Maksim Sipos. *Unsuitability of NOTEARS for causal graph discovery*. arXiv preprint arXiv:2104.05441 (2021).

[37] Zheng, Xun, et al. *Dags with no tears: Continuous optimization for structure learning*. Advances in Neural Information Processing Systems 31 (2018).

[38] Dinh, Laurent, Jascha Sohl-Dickstein, and Samy Bengio. *Density estimation using real nvp*. arXiv preprint arXiv:1605.08803 (2016).

Appendix A COMPLETE EXPERIMENTAL RESULTS OF CAUSAL DISCOVERY

Table 1: The Complete Results of Heuristic Causal Discovery in latent space. Each row stands for a round of detection, with ‘#’ identifying the round number, and all candidate edges are listed with their KLD gains as below. 1) Green cells: the newly detected edges. 2) Red cells: the selected edge. 3) Blue cells: the trimmed edges accordingly.

#	1	A \rightarrow C	A \rightarrow D	A \rightarrow E	A \rightarrow F	B \rightarrow C	B \rightarrow D	B \rightarrow E	B \rightarrow F	C \rightarrow F	C \rightarrow G	C \rightarrow H	C \rightarrow I
# 2	7.6354	19.7407	60.1876	60.1876	119.7730	8.5147	65.9335	132.7717	8.5147	65.9335	132.7717	95.1564	
# 3	9.7357	19.7407	60.1876	A \rightarrow E	B \rightarrow D	B \rightarrow E	B \rightarrow F	C \rightarrow D	C \rightarrow E	C \rightarrow F	C \rightarrow G	C \rightarrow H	C \rightarrow I
# 4	60.1876	119.7730	65.9335	132.7717	1.13355	46.5876	111.2978	10.1490	46.5876	111.2978	11.6012	39.2361	25.1988
# 5	60.1876	119.7730	65.9335	132.7717	46.5876	111.2978	11.6012	39.2361	95.1564	63.7348	123.3203	27.8798	75.5795
# 6	60.1876	119.7730	65.9335	132.7717	46.5876	111.2978	11.6012	39.2361	95.1564	63.7348	123.3203	27.8798	25.1988
# 7	60.1876	119.7730	65.9335	132.7717	46.5876	111.2978	11.6012	39.2361	95.1564	63.7348	123.3203	27.8798	25.1988
# 8	60.1876	119.7730	65.9335	132.7717	46.5876	111.2978	11.6012	39.2361	95.1564	63.7348	123.3203	27.8798	25.1988
# 9	60.1876	119.7730	65.9335	132.7717	46.5876	111.2978	11.6012	39.2361	95.1564	63.7348	123.3203	27.8798	25.1988
# 10	119.7730	-6.8372	132.7717	111.2978	95.1564	17.0407	123.3203	75.5775	53.6806	-5.9191		-3.2931	110.2558
# 11	119.7730	A \rightarrow F	B \rightarrow F	C \rightarrow F	C \rightarrow I	D \rightarrow F	D \rightarrow I	E \rightarrow F	E \rightarrow G	E \rightarrow H	E \rightarrow I		
# 12	119.7730	132.7717	111.2978	95.1564	123.3203	75.5775	53.6806	-5.9191	-3.2931	110.2558			
# 13	119.7730	132.7717	111.2978	95.1564	123.3203	75.5775	53.6806	-5.9191	-3.2931	110.2558			
# 14	C \rightarrow I	D \rightarrow I	E \rightarrow I	F \rightarrow I									
# 15	95.1564	75.5775	110.2558	45.6490									
# 16	15.0222	C \rightarrow I	D \rightarrow I	I \rightarrow J									
		3.3845	D \rightarrow I	0.0284									
		15.0222	3.3845										

Table 2: Average performance of 10-Fold FGES (Fast Greedy Equivalence Search) causal discovery, with the prior knowledge that each node can only cause the other nodes with the same or greater depth with it. An edge means connecting two attributes from two different nodes, respectively. Thus, the number of possible edges between two nodes is the multiplication of the numbers of their attributes, i.e., the lengths of their data vectors.

Table 3: Brief Results of the Heuristic Causal Discovery in latent space, identical with Table 3 in the paper body, for better comparison to the traditional FGES methods results on this page.
 The edges are arranged in detected order (from left to right) and their measured causal strengths in each step are shown below correspondingly.

Causation	A→C	B→D	C→D	C→G	D→G	G→J	D→H	H→J	C→E	B→E	E→G	E→H	E→F	F→I	I→J	D→I
KLD	7.63	8.51	10.14	11.60	27.87	5.29	25.19	15.93	46.58	65.93	39.13	39.88	53.68	45.64	17.41	75.57
Gain	7.63	8.51	1.135	11.60	2.454	5.29	25.19	0.209	46.58	-6.84	-5.91	-3.29	53.68	45.64	0.028	3.384